Available online at https://jcupt.bupt.edu.cn

The Journal of China Universities of Posts and Telecommunications

April 2025, 32(2): 70 – 81

Hybrid precoding schemes for mmWave massive MIMO V2V system with finite-resolution PSs

Liang Xiaolin[1,2], Rong Zhanyi[1] (✉), Cao Wangbin[3]

1. College of Electronic and Information Engineering, Hebei University, Baoding 071002, China
2. Hebei Key Laboratory of Power Internet of Things Technology, North China Electric Power University, Baoding 071003, China
3. School of Electrical and Electronic Engineering, North China Electric Power University, Baoding 071003, China

Abstract

Considering the significant expenses and power requirements associated with digital precoding and the low spectral efficiency (SE) of analog precoding, a hybrid precoding algorithm with efficient finite-resolution phase shifters (PSs), named FRPS algorithm, was proposed for millimeter wave (mmWave) massive multi-input multi-output (MIMO) vehicle-to-vehicle (V2V) system. Digital and analog precoding matrix variables and non-convex constraints of the radio frequency (RF) precoder are decomposed into two independent optimization problems. Discrete iterative optimization is employed to solve for the analog and digital precoder alternately. In addition, the effect of finite-resolution PSs is considered in the precoding algorithm optimization. Simulation results show that the FRPS algorithm has a fast convergence speed, and it can approach the SE of fully digital precoding with only 3 bit resolution PS. The performance difference between the FRPS algorithm and the existing hybrid precoding algorithm with infinite-resolution PSs is almost negligible. Moreover, the FRPS algorithm performs superior to that of the infinite-resolution PS hybrid precoding algorithm and fully digital precoding algorithm.

Keywords hybrid precoding, millimeter wave (mmWave) communication, vehicle-to-vehicle (V2V) communication, finite-resolution phase shifters, massive multi-input multi-output (MIMO)

1 Introduction

V2V communication brings profound changes that greatly enhance user experience and improve road safety in the 6th-generation mobile communication (6G) era[1]. As one of the fundamental technologies for intelligent transport systems and autonomous driving[2], V2V communication necessitates elevated standards for quality of service (QoS) and reliability[3]. Emerging smart transportation and autonomous driving systems require significantly higher bandwidth and data rates than those currently supported by sub-6GHz vehicle-to-everything (V2X) technologies. This triggers interest in developing multiple antenna technologies and mmWave precoding schemes that enable V2V communication to transmit data in the desired direction[4].

The mmWave communication has the characteristics of large bandwidth, strong directionality, and exact signal delivery. It is vital for solving the problem of

Special Issue: The 27th Annual Meeting of The China Association for Science and Technology

Corresponding author: Rong Zhanyi, E-mail: rongzhanyi1@163.com

DOI: 10.19682/j.cnki.1005-8885.2025.0017

insufficient bandwidth in current mobile communication systems[5-6]. Despite challenges such as path loss and weather-related interference[7], mmWave signals enable the integration of a large number of antenna elements into a small form factor[8]. Merging mmWave transmission with massive MIMO is a widely discussed issue[9]. Large-scale antenna arrays on vehicle transceivers help to mitigate the path and penetration losses in the mmWave band [10].

The mmWave MIMO precoding is used in V2V systems to provide significant beamforming gains. A digital precoder is usually used for traditional MIMO precoding. However, if a digital precoder is used, each antenna requires a separate RF chain. The increase of the RF chain will bring exorbitant costs and energy expenditure[11]. Analog precoders implemented through PS can solely manipulate the signal phase, resulting in significant performance degradation. In mmWave massive MIMO systems, hybrid precoding has emerged as a promising approach, capable of achieving performance comparable to fully digital precoders, while significantly reducing the number of required RF chains[12-15].

In hybrid precoding, the transmitting and receiving analog and digital precoders are coupled. This coupling renders the optimized objective function non-convex and arduous to solve[16]. To address the non-convex challenge, hybrid precoding can be reformulated as a matrix factorization issue. The Euclidean distance between hybrid and fully digital precoding is then minimized. Using the sparsity of mmWave channels and the orthogonal matching pursuit (OMP) method, an approximate optimal unconstrained precoding algorithm was proposed in Ref. [17]. A manifold optimization based alternating minimization (MO-AltMin) algorithm was proposed in Ref. [18]. Initially, the method breaks down the primary issue into combinations involving hybrid precoding and subproblems, subsequently concentrates on resolving the constant modulus limitations within these subproblems. In Ref. [19], practical yet efficient statistically-aided codebook-based hybrid precoding schemes were presented, which require lower channel feedback overhead.

The above precoder designs all assume infinite-resolution PSs. However, the infinite-resolution PS design is challenging and finite-resolution PSs are often used in practice. When the hybrid precoder uses 1 bit PS, the precoding problem takes on a lattice structure. According to lattice theory, the mean square error performance gap between the fully and hybrid precoder/combiner under the 1 bit PS constraint was deduced in Ref. [20]. An analog precoder and FRPS combination scheme for multiuser MIMO systems was proposed in Ref. [21], which reformulated the analog precoder and combiner design problem as a phase categorization problem. A general neural network architecture was also proposed. A FRPS algorithm with low transmitting power was presented in Ref. [22], which achieves satisfactory performance in partially connected structures. An iterative phase matching algorithm was proposed in Ref. [23]. Findings demonstrate that the iterative phase matching algorithm can enhance SE in scenarios with finite-resolution.

Investigations on hybrid precoding are mostly for traditional cellular networks. Although mmWave has been extensively utilized in static scenarios, it is still a major challenge to apply mmWave hybrid precoding in high-speed mobile scenarios, because the transceiver moves at high-speed and the channel is different from the static channel[7]. Unmanned aerial vehicle hybrid beamforming for massive MIMO was investigated in Ref. [24], and an approximate closed-form expression for the rate was derived. A reinforcement learning algorithm utilizing the deep deterministic policy gradient method was proposed in Ref. [25]. The algorithm is used to optimize base station (BS) and intelligent reflecting surface (IRS) beamforming to improve vehicle-to-infrastructure (V2I) communication performance. The comprehensive analysis of V2V networks in mmWave was conducted in Ref. [26], and the results demonstrate that proper precoding design can ensure higher communication performance. A MIMO hybrid beamforming combined with a time difference of arrival (TDOA)/frequency difference of arrival (FDOA) mmWave vehicle location method was proposed in Ref. [27]. Most existing work on V2V hybrid precoding assumes the utilization of infinite-

resolution PSs, which is unrealistic. Therefore, the hybrid precoding schemes with finite-resolution PSs for mmWave massive MIMO V2V system need further investigation.

To make up for these deficiencies, a hybrid precoding scheme for mmWave massive MIMO V2V system with finite-resolution PSs, FRPS algorithm, is proposed. The digital and analog precoders are collaboratively designed to enhance SE and energy efficiency (EE). The concept of iterative optimization in discrete form is deployed to tackle the analog and digital precoders alternately. A two-stage iterative hybrid precoding algorithm based on finite-resolution PSs is proposed. The main contributions of this paper are summarized as follows.

1) FRPS algorithm is proposed for mmWave massive MIMO V2V system, and it performs well for high-speed mobility scenarios. In order to derive the digital and analog precoding matrix variables and meet the non-convex constraints of the RF precoder, the issue is decomposed into two independent optimization problems, and discrete iterative optimization is employed to alternate optimization between the analog and digital precoders.

2) Aiming to optimize the EE of the algorithm, and avoid the complicated design of infinite-resolution PS, the low-precision quantization model is considered in designing the hybrid precoding algorithm. Then the objective function of hybrid precoding for mmWave massive MIMO V2V system can be simplified to a closed-form solution.

3) The FRPS algorithm is compared to the existing hybrid, analog, and fully digital precoding algorithms. The findings indicate that the algorithm exhibits swift convergence and can improve the SE and EE effectively. Moreover, the FRPS algorithm does not need a large PS resolution, and the system performance can achieve the best when 3 bit resolution PS.

The rest of this paper is organized as follows. Sect. 2 describes the V2V system and channel model. In Sect. 3, the mmWave massive MIMO FRPS algorithm in V2V system is described. Sect. 4 displays the experimental results and comparative analysis of the results. Finally, the conclusions are drawn in Sect. 5.

Notation: $\boldsymbol{A}$ is a matrix, $\boldsymbol{a}$ is a vector. $A_{m,n}$ is the entry on the mth row and nth column of a matrix. $\mathbb{R}$ and $\mathbb{C}$ to represent the set of real numbers and complex numbers, respectively. $(\cdot)^*$, $(\cdot)^{\mathrm{T}}$, and $(\cdot)^{\mathrm{H}}$ stands for the conjugate, transpose, and conjugate transpose, respectively. $\det(\cdot)$ and $\|\cdot\|_{\mathrm{F}}$ denote the determinant and Frobenius norm. $\mathrm{tr}(\cdot)$ and $\mathrm{vec}(\cdot)$ indicate the trace and vectorization; $(\cdot)^{\dagger}$ is the Moore-Penrose pseudo inverse. $\mathbb{E}[\cdot]$ denotes the expectation operator. Real part of a complex variable is noted by $\mathrm{Re}[\cdot]$. $\circ$ and $\otimes$ denote the Hadamard and Kronecker products between two matrices.

2 System and channel model

In this section, the mmWave massive MIMO V2V system model and the mmWave channel model with mobility are introduced.

2.1 System model

A mmWave massive MIMO V2V system using a hybrid precoder and combiner with finite-resolution PSs is considered, as shown in Fig. 1. Equipped with M_{T} antenna elements and $M_{\mathrm{T}}^{\mathrm{RF}}$ RF chains, the transmitting vehicle user equipment (t-VUE) is capable of simultaneously dispatching N_{s} data streams via the mmWave channel to the receiving vehicle user equipment (r-VUE). The r-VUE is equipped with M_{R} antenna elements and $M_{\mathrm{R}}^{\mathrm{RF}}$ RF chains. The conditions $N_{\mathrm{s}} \leqslant M_{\mathrm{T}}^{\mathrm{RF}} \leqslant M_{\mathrm{T}}$ and $N_{\mathrm{s}} \leqslant M_{\mathrm{R}}^{\mathrm{RF}} \leqslant M_{\mathrm{R}}$ are established to facilitate multi-stream transmission, while minimizing the RF chain count.

At the t-VUE, the digital precoder $\boldsymbol{P}_{\mathrm{D}}$ is firstly applied to process the N_{s} data streams represented by vector $\boldsymbol{s}$ with $\mathbb{E}[\boldsymbol{s}\boldsymbol{s}^{\mathrm{H}}] = (1/N_{\mathrm{s}})\boldsymbol{I}_{N_{\mathrm{s}}}$, $\boldsymbol{I}_{N_{\mathrm{s}}}$ represents the identity matrix. To enhance beamforming performance, an analog precoder $\boldsymbol{P}_{\mathrm{RF}}$ made up of adjustable PSs is used before the RF signals are emitted by its M_{T} antennas. Therefore, the transmitted signal can be expressed as $\boldsymbol{x} = \boldsymbol{P}_{\mathrm{RF}}\boldsymbol{P}_{\mathrm{D}}\boldsymbol{s}$. So, the hybrid precoders $\boldsymbol{P} = \boldsymbol{P}_{\mathrm{RF}}\boldsymbol{P}_{\mathrm{D}} \in \mathbb{C}^{M_{\mathrm{T}} \times N_{\mathrm{s}}}$, where $\boldsymbol{P}_{\mathrm{D}} \in \mathbb{C}^{M_{\mathrm{T}}^{\mathrm{RF}} \times N_{\mathrm{s}}}$ and $\boldsymbol{P}_{\mathrm{RF}} \in$

$\mathbb{C}^{M_T \times M_T^{RF}}$. Moreover, the normalized transmit power constraint is expressed as $\| \boldsymbol{P}_{RF}\boldsymbol{P}_D \|_F^2 = N_s$. Similarly, the r-VUE employs a hybrid combiner $\boldsymbol{Q} = \boldsymbol{Q}_{RF}\boldsymbol{Q}_D \in \mathbb{C}^{M_R \times N_s}$ to handle the incoming signal, where $\boldsymbol{Q}_D \in \mathbb{C}^{M_T^{RF} \times N_s}$ and $\boldsymbol{Q}_{RF} \in \mathbb{C}^{M_R \times M_T^{RF}}$ are the digital combiner and the analog combiner, respectively. The analog combiner $\boldsymbol{Q}_{RF}$ is likewise realized through an set of adjustable PSs. Thus, the received signal is presented as

$$\boldsymbol{y} = \sqrt{\rho}\boldsymbol{Q}_D^H\boldsymbol{Q}_{RF}^H\boldsymbol{H}\boldsymbol{P}_{RF}\boldsymbol{P}_D\boldsymbol{s} + \boldsymbol{Q}_D^H\boldsymbol{Q}_{RF}^H\boldsymbol{u} \tag{1}$$

where ρ denotes the average received power, $\boldsymbol{H} \in \mathbb{C}^{M_R \times M_T}$ denotes the mmWave massive MIMO channel matrix, and $\boldsymbol{u} \in \mathbb{C}^{M_R}$ represents additive Gaussian noise vector whose entries are independent and identically distributed (i. i. d.) as $\mathcal{CN}(0, \sigma_u^2)$. It is presumed that comprehensive channel state information (CSI) is accessible to both the transmitter (Tx) and receiver (Rx)[18,27].

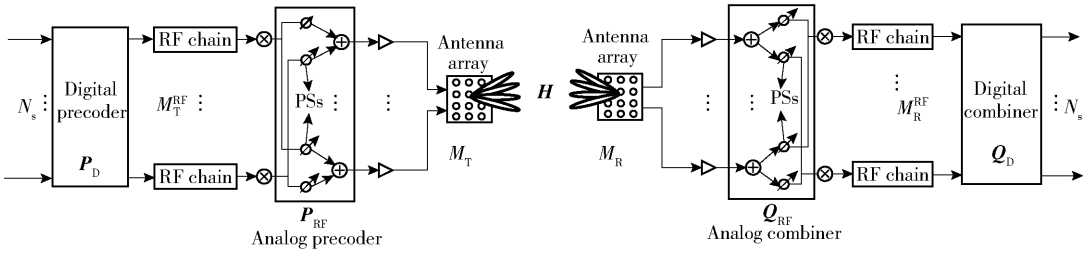

Fig. 1 Structures of hybrid precoding for mmWave massive MIMO V2V system

2.2 Channel model

A mmWave massive MIMO V2V network scenario is considered. Specifically, to account for a practical environment, each VUE has the functionality to establish a directional beam, facilitating the conveyance of signals to a counterpart VUE. One acts as a Tx and the other acts as a Rx.

The Saleh-Valenzuela (SV) channel model[28] is considered, which is a conventional channel model in the case of mmWave massive MIMO systems. In addition, the Doppler shifts are further considered because of the mobility of V2V systems. The mmWave propagation channel is characterized by a geometry-based channel model. It is delineated by N_C, each composed of N_R rays. The $M_R \times M_T$ channel matrix $\boldsymbol{H}$ can be represented as

$$\boldsymbol{H}(t,\tau) = \sqrt{\frac{M_T M_R}{N_C N_R}} \sum_{i=1}^{N_C}\sum_{l=1}^{N_R} \alpha_{il}\boldsymbol{a}_r(\phi_{il}^r, \theta_{il}^r)\boldsymbol{a}_t^H(\phi_{il}^t, \theta_{il}^t) \cdot \delta(\tau - \tau_{il})\mathrm{e}^{-\mathrm{j}2\pi v_{il}t} \tag{2}$$

where t denotes time slot and τ denotes time delay, α_{il} denotes the gain of the lth ray in the ith propagation cluster. α_{il} is assumed to be i. i. d. and follow the distribution $\mathcal{CN}(0, \sigma_{\alpha,i}^2)$, where $\sigma_{\alpha,i}^2$ is the average power of the ith cluster with $\sum_{i=1}^{N_C}\sigma_{\alpha,i}^2 \triangleq \Gamma$, Γ is a normalization factor for ensuring that $\mathbb{E}[\| \boldsymbol{H} \|_F^2] = M_T M_R$. In addition, $\boldsymbol{a}_r(\phi_{il}^r, \theta_{il}^r)$ and $\boldsymbol{a}_t(\phi_{il}^t, \theta_{il}^t)$ represent the receiving and transmitting array response vectors, where ϕ_{il}^r, ϕ_{il}^t, θ_{il}^r, θ_{il}^t stand for azimuthal angle of arrival (AoA), azimuthal angle of departure (AoD), elevational AoA, and elevational AoD of the lth path in the ith cluster, respectively. The azimuth and elevation AoAs and AoDs follow the Laplacian distribution. Uniform planar arrays (UPA) with $\sqrt{M} \times \sqrt{M}$ antenna elements of mmWave systems are considered. The vector that represents the array response for the lth ray within the ith cluster can be written as

$$\boldsymbol{a}(\phi_{il}, \theta_{il}) = \frac{1}{\sqrt{M}}[1, \mathrm{e}^{\mathrm{j}\frac{2\pi}{\lambda}d(p\sin\phi_{il}\sin\theta_{il} + q\cos\theta_{il})}, \ldots, \mathrm{e}^{\mathrm{j}\frac{2\pi}{\lambda}d((\sqrt{M}-1)\sin\phi_{il}\sin\theta_{il} + (\sqrt{M}-1)\cos\theta_{il})}]^T \tag{3}$$

where d denotes the antenna spacing and λ represents the wavelength of the signal. $0 \leqslant p < \sqrt{M}$ and $0 \leqslant q < \sqrt{M}$ are element indices. UPAs are used at both t-VUE and r-VUE. A two-dimensional (2D) coordinate system is considered where the position of t-VUE is at the origin $(0,0)$. It is assumed that both the t-VUE and the r-VUE are moving along the horizontal axis with speed v^{Tx} and v^{Rx}, respectively.

The propagation delay for the (i,l)th path is given

by $\tau_{il}=r_{il}/\mathrm{c}$, with c being the velocity of light and r_{il} is the propagation length with the (i,l)th path. It can be obtained as

$$r_{il}=r_i+\sqrt{(r_i\sin\theta_{il}^{\mathrm{t}})^2+(D-r_i\cos\theta_{il}^{\mathrm{t}}\cos\phi_{il}^{\mathrm{t}})^2} \tag{4}$$

where r_i is the distance from the Tx of the scatterer in the ith cluster and D is the distance between the t-VUE and r-VUE. Doppler shifts v_{il} can be obtained as

$$v_{il}=-\frac{f}{\mathrm{c}}(v^{\mathrm{Rx}}\cos\theta_{il}^{\mathrm{r}}\cos\phi_{il}^{\mathrm{r}}+v^{\mathrm{Tx}}\cos\theta_{il}^{\mathrm{t}}\cos\phi_{il}^{\mathrm{t}}) \tag{5}$$

where f is the carrier frequency.

3 FRPS algorithm

3.1 Problem formulation

Practical and hardware-efficient scenarios are considered in which the PSs have finite-resolution to reduce the power consumption and complexity. Within this constraint, the mmWave massive MIMO hybrid precoding algorithms for V2V systems to maximize SE are designed. When Gaussian signals are conveyed via mmWave MIMO channels, the SE can be achieved as

$$R(\boldsymbol{P}_{\mathrm{D}},\boldsymbol{P}_{\mathrm{RF}},\boldsymbol{Q}_{\mathrm{D}},\boldsymbol{Q}_{\mathrm{RF}})=\mathrm{lb}\ \det\left(\boldsymbol{I}_{N_{\mathrm{s}}}+\frac{\rho}{\sigma_{\boldsymbol{u}}^2N_{\mathrm{s}}}\cdot(\boldsymbol{Q}_{\mathrm{RF}}\boldsymbol{Q}_{\mathrm{D}})^{\dagger}\boldsymbol{H}\boldsymbol{P}_{\mathrm{RF}}\boldsymbol{P}_{\mathrm{D}}\boldsymbol{P}_{\mathrm{D}}^{\mathrm{H}}\boldsymbol{P}_{\mathrm{RF}}^{\mathrm{H}}\boldsymbol{H}^{\mathrm{H}}(\boldsymbol{Q}_{\mathrm{RF}}\boldsymbol{Q}_{\mathrm{D}})\right) \tag{6}$$

Given finite-resolution PSs and subject to a total power constraint at the Tx, the problem of hybrid precoding design can be articulated as

$$\left.\begin{aligned}&\max_{\boldsymbol{P}_{\mathrm{D}},\boldsymbol{P}_{\mathrm{RF}},\boldsymbol{Q}_{\mathrm{D}},\boldsymbol{Q}_{\mathrm{RF}}} R(\boldsymbol{P}_{\mathrm{D}},\boldsymbol{P}_{\mathrm{RF}},\boldsymbol{Q}_{\mathrm{D}},\boldsymbol{Q}_{\mathrm{RF}})\\&\text{s. t.}\\&\quad\|\boldsymbol{P}_{\mathrm{RF}}\boldsymbol{P}_{\mathrm{D}}\|_{\mathrm{F}}^2=N_{\mathrm{s}}\\&\quad P_{\mathrm{RF}m,n}\in\mathscr{A};\quad\forall m,n\\&\quad Q_{\mathrm{RF}m,n}\in\mathscr{A};\quad\forall m,n\end{aligned}\right\} \tag{7}$$

where $\mathscr{A}$ is a feasible set of simulated beamforming matrices at the transmitting and receiving ends. The constraint $\mathscr{A}$ is defined by the finite-resolution PSs. To solve Eq. (7), a joint optimization over the four matrix variables $\boldsymbol{P}_{\mathrm{D}}$, $\boldsymbol{P}_{\mathrm{RF}}$, $\boldsymbol{Q}_{\mathrm{D}}$, and $\boldsymbol{Q}_{\mathrm{RF}}$ is required. The data stream first passes through the digital precoder $\boldsymbol{P}_{\mathrm{D}}$ and then through the analog precoder $\boldsymbol{P}_{\mathrm{RF}}$ to get the transmission signal $\boldsymbol{x}=\boldsymbol{P}_{\mathrm{RF}}\boldsymbol{P}_{\mathrm{D}}\boldsymbol{s}$. After the receiver sends the signal through the channel, it passes through the analog combiner $\boldsymbol{Q}_{\mathrm{RF}}$ and the digital combiner $\boldsymbol{Q}_{\mathrm{D}}$, and finally gets the received signal $\boldsymbol{y}$. The design of $\boldsymbol{P}_{\mathrm{RF}}$ incorporates finite-resolution PSs, which restricts their functionality to phase alteration of signals. The values of each PS are discretized into a finite set, as explained in the next section.

Optimizing Eq. (7) is challenging due to the simultaneous refinement of four matrices, coupled with the non-convex limitations inherent in the RF precoder and combiner. The problems mentioned can be decomposed into two separate optimization problems: the precoding and decoding problems. This decomposition simplifies the design process for the joint hybrid precoding and decoding. While hybrid precoding incorporates extra power constraints, its mathematical formulations share a resemblance with those utilized in decoding problems. Therefore, the design of the precoder will be highlighted.

The hybrid precoding design problem formulation is given by

$$\left.\begin{aligned}&\min_{\boldsymbol{P}_{\mathrm{D}},\boldsymbol{P}_{\mathrm{RF}}}\|\boldsymbol{P}_{\mathrm{opt}}-\boldsymbol{P}_{\mathrm{RF}}\boldsymbol{P}_{\mathrm{D}}\|_{\mathrm{F}}\\&\text{s. t.}\\&\quad\|\boldsymbol{P}_{\mathrm{RF}}\boldsymbol{P}_{\mathrm{D}}\|_{\mathrm{F}}^2=N_{\mathrm{s}}\\&\quad P_{\mathrm{RF}m,n}\in\mathscr{A};\quad\forall m,n\end{aligned}\right\} \tag{8}$$

where $\boldsymbol{P}_{\mathrm{D}}$ and $\boldsymbol{P}_{\mathrm{RF}}$ are the digital and analog precoders to be optimized. $\boldsymbol{P}_{\mathrm{opt}}$ stands for the optimal fully digital precoder. It consists of the first N_{s} columns from both the matrices $\boldsymbol{V}$ and $\boldsymbol{U}$, where $\boldsymbol{V}$ and $\boldsymbol{U}$ is obtained by singular value decomposition (SVD) of the channel, that is, $\boldsymbol{H}=\boldsymbol{U}\sum\boldsymbol{V}^{\mathrm{H}}$. However, Eq. (8) that is no simple closed-form solutions exist because of the coupled $\boldsymbol{P}_{\mathrm{RF}}$ and $\boldsymbol{P}_{\mathrm{D}}$ as well as the non-convex constraint are set with finite-resolution PSs.

It has been proved that approximate minimization of the objective function in Eq. (8) can maximize the SE[17]. In order to obtain better SE and EE, the digital and analog precoder are jointly designed, and the discrete iterative optimization idea is used to solve the analog and digital precoder alternately. In addition, the influence of discrete phase values should also be considered during optimization.

3.2 FRPS algorithm

It first considers designing the digital precoding

matrix $\boldsymbol{P}_{\mathrm{D}}$. Thus Eq. (8) can be reformulated as

$$\min_{\boldsymbol{P}_{\mathrm{D}}} \| \boldsymbol{P}_{\mathrm{opt}} - \boldsymbol{P}_{\mathrm{RF}}\boldsymbol{P}_{\mathrm{D}} \|_{\mathrm{F}} \tag{9}$$

Eq. (9) are known to have least squares solutions. Thus, $\boldsymbol{P}_{\mathrm{D}}$ can be obtained as

$$\boldsymbol{P}_{\mathrm{D}} = (\boldsymbol{P}_{\mathrm{RF}})^{\dagger}\boldsymbol{P}_{\mathrm{opt}} \tag{10}$$

Next, the design of the analog precoder will be highlighted. Applying a constraint to a digital precoding matrix, that is, the columns of the $\boldsymbol{P}_{\mathrm{D}}$ should be mutually orthogonal, i. e., $\boldsymbol{P}_{\mathrm{D}}^{\mathrm{H}}\boldsymbol{P}_{\mathrm{D}} = \beta\boldsymbol{P}_{\mathrm{B}}^{\mathrm{H}}\beta\boldsymbol{P}_{\mathrm{B}} = \beta^2\boldsymbol{I}_{N_s}$, where $\boldsymbol{P}_{\mathrm{B}}$ is a unitary matrix with the same dimension as $\boldsymbol{P}_{\mathrm{D}}$, β is a constraint variable. This is inspired by the unconstrained precoding solution. Orthogonal constraints are pivotal in the design of analog precoders, as they can substantially streamline the complexity. By replacing $\boldsymbol{P}_{\mathrm{D}}$ with $\beta\boldsymbol{P}_{\mathrm{B}}$ in Eq. (8), the objective function can be further written as

$$\begin{aligned}
&\| \boldsymbol{P}_{\mathrm{opt}} - \boldsymbol{P}_{\mathrm{RF}}\boldsymbol{P}_{\mathrm{D}} \|_{\mathrm{F}}^2 = \| \boldsymbol{P}_{\mathrm{opt}} - \boldsymbol{P}_{\mathrm{RF}}\beta\boldsymbol{P}_{\mathrm{B}} \|_{\mathrm{F}}^2 = \\
&\quad \| \boldsymbol{P}_{\mathrm{opt}} \|_{\mathrm{F}}^2 - \beta\mathrm{tr}(\boldsymbol{P}_{\mathrm{opt}}^{\mathrm{H}}\boldsymbol{P}_{\mathrm{RF}}\boldsymbol{P}_{\mathrm{B}}) - \\
&\quad \beta\mathrm{tr}(\boldsymbol{P}_{\mathrm{B}}^{\mathrm{H}}\boldsymbol{P}_{\mathrm{RF}}^{\mathrm{H}}\boldsymbol{P}_{\mathrm{opt}}) + \beta^2 \| \boldsymbol{P}_{\mathrm{RF}}\boldsymbol{P}_{\mathrm{B}} \|_{\mathrm{F}}^2 = \\
&\quad \| \boldsymbol{P}_{\mathrm{opt}} \|_{\mathrm{F}}^2 - 2\beta\mathrm{Re\ Tr}(\boldsymbol{P}_{\mathrm{B}}\boldsymbol{P}_{\mathrm{opt}}^{\mathrm{H}}\boldsymbol{P}_{\mathrm{RF}}) + \\
&\quad \beta^2 \| \boldsymbol{P}_{\mathrm{RF}}\boldsymbol{P}_{\mathrm{B}} \|_{\mathrm{F}}^2
\end{aligned} \tag{11}$$

when $\beta = \mathrm{Re\ tr}(\boldsymbol{P}_{\mathrm{B}}\boldsymbol{P}_{\mathrm{opt}}^{\mathrm{H}}\boldsymbol{P}_{\mathrm{RF}}) / \| \boldsymbol{P}_{\mathrm{RF}}\boldsymbol{P}_{\mathrm{B}} \|_{\mathrm{F}}^2$, the objective function has the minimum value, and can be given by

$$\| \boldsymbol{P}_{\mathrm{opt}} \|_{\mathrm{F}}^2 - \frac{\{\mathrm{Re\ tr}(\boldsymbol{P}_{\mathrm{B}}\boldsymbol{P}_{\mathrm{opt}}^{\mathrm{H}}\boldsymbol{P}_{\mathrm{RF}})\}^2}{\| \boldsymbol{P}_{\mathrm{RF}}\boldsymbol{P}_{\mathrm{B}} \|_{\mathrm{F}}^2} \tag{12}$$

It should be noted that $\| \boldsymbol{P}_{\mathrm{RF}}\boldsymbol{P}_{\mathrm{B}} \|_{\mathrm{F}}^2$ has the following upper bound

$$\begin{aligned}
\| \boldsymbol{P}_{\mathrm{RF}}\boldsymbol{P}_{\mathrm{B}} \|_{\mathrm{F}}^2 &= \mathrm{tr}(\boldsymbol{P}_{\mathrm{B}}^{\mathrm{H}}\boldsymbol{P}_{\mathrm{RF}}^{\mathrm{H}}\boldsymbol{P}_{\mathrm{RF}}\boldsymbol{P}_{\mathrm{B}}) = \\
&\quad \mathrm{tr}\left(\begin{pmatrix} \boldsymbol{I}_{N_s} & \\ & \boldsymbol{0} \end{pmatrix}\boldsymbol{L}^{\mathrm{H}}\boldsymbol{P}_{\mathrm{RF}}^{\mathrm{H}}\boldsymbol{P}_{\mathrm{RF}}\boldsymbol{L}\right) \leqslant \\
&\quad \mathrm{tr}(\boldsymbol{L}^{\mathrm{H}}\boldsymbol{P}_{\mathrm{RF}}^{\mathrm{H}}\boldsymbol{P}_{\mathrm{RF}}\boldsymbol{L}) = \| \boldsymbol{P}_{\mathrm{RF}} \|_{\mathrm{F}}^2
\end{aligned} \tag{13}$$

where $\boldsymbol{P}_{\mathrm{B}}\boldsymbol{P}_{\mathrm{B}}^{\mathrm{H}} = \boldsymbol{L}\begin{pmatrix} \boldsymbol{I}_{N_s} & \\ & \boldsymbol{0} \end{pmatrix}\boldsymbol{L}^{\mathrm{H}}$ is the SVD of $\boldsymbol{P}_{\mathrm{B}}\boldsymbol{P}_{\mathrm{B}}^{\mathrm{H}}$ and the equality holds when $M_{\mathrm{T}}^{\mathrm{RF}} = N_s$, i. e., $\boldsymbol{P}_{\mathrm{B}}$ is a square matrix. Hence, Eq. (12) can be written as $\| \boldsymbol{P}_{\mathrm{opt}} \|_{\mathrm{F}}^2 - \{\mathrm{Re\ tr}(\boldsymbol{P}_{\mathrm{B}}\boldsymbol{P}_{\mathrm{opt}}^{\mathrm{H}}\boldsymbol{P}_{\mathrm{RF}})\}^2 / \| \boldsymbol{P}_{\mathrm{RF}} \|_{\mathrm{F}}^2$, where $\boldsymbol{P}_{\mathrm{B}}$ and $\boldsymbol{P}_{\mathrm{RF}}$ are coupled, and it is very complicated to optimize the two variables jointly. In order to rid $\boldsymbol{P}_{\mathrm{RF}}$ of the product of $\boldsymbol{P}_{\mathrm{B}}$, the following transformation is performed.

Let's add the constant term to $\| \boldsymbol{P}_{\mathrm{opt}} \|_{\mathrm{F}}^2 - \{\mathrm{Re\ tr}(\boldsymbol{P}_{\mathrm{B}}\boldsymbol{P}_{\mathrm{opt}}^{\mathrm{H}}\boldsymbol{P}_{\mathrm{RF}})\}^2 / \| \boldsymbol{P}_{\mathrm{RF}} \|_{\mathrm{F}}^2$ and multiply it by a positive constant term to get $(\| \boldsymbol{P}_{\mathrm{opt}} \|_{\mathrm{F}}^2 - \{\mathrm{Re\ tr}(\boldsymbol{P}_{\mathrm{B}}\boldsymbol{P}_{\mathrm{opt}}^{\mathrm{H}}\boldsymbol{P}_{\mathrm{RF}})\}^2 / \| \boldsymbol{P}_{\mathrm{RF}} \|_{\mathrm{F}}^2 + \| \boldsymbol{P}_{\mathrm{opt}} \|_{\mathrm{F}}^2 / (2 \cdot \| \boldsymbol{P}_{\mathrm{RF}} \|_{\mathrm{F}}^2) - \| \boldsymbol{P}_{\mathrm{opt}} \|_{\mathrm{F}}^2 + 1/2) \times 2 \| \boldsymbol{P}_{\mathrm{RF}} \|_{\mathrm{F}}^2$. Then it have

$$\begin{aligned}
&\left(\| \boldsymbol{P}_{\mathrm{opt}} \|_{\mathrm{F}}^2 - \frac{\{\mathrm{Re\ tr}(\boldsymbol{P}_{\mathrm{B}}\boldsymbol{P}_{\mathrm{opt}}^{\mathrm{H}}\boldsymbol{P}_{\mathrm{RF}})\}^2}{\| \boldsymbol{P}_{\mathrm{RF}} \|_{\mathrm{F}}^2} + \frac{\| \boldsymbol{P}_{\mathrm{opt}} \|_{\mathrm{F}}^2}{2 \| \boldsymbol{P}_{\mathrm{RF}} \|_{\mathrm{F}}^2} - \right. \\
&\quad \left. \| \boldsymbol{P}_{\mathrm{opt}} \|_{\mathrm{F}}^2 + \frac{1}{2} \right) \times 2 \| \boldsymbol{P}_{\mathrm{RF}} \|_{\mathrm{F}}^2 = \| \boldsymbol{P}_{\mathrm{opt}} \|_{\mathrm{F}}^2 - \\
&\quad 2\mathrm{Re\ tr}(\boldsymbol{P}_{\mathrm{B}}\boldsymbol{P}_{\mathrm{opt}}^{\mathrm{H}}\boldsymbol{P}_{\mathrm{RF}}) + \| \boldsymbol{P}_{\mathrm{RF}} \|_{\mathrm{F}}^2 = \\
&\quad \mathrm{tr}(\boldsymbol{P}_{\mathrm{RF}}^{\mathrm{H}}\boldsymbol{P}_{\mathrm{RF}}) - 2\mathrm{Re\ tr}(\boldsymbol{P}_{\mathrm{B}}\boldsymbol{P}_{\mathrm{opt}}^{\mathrm{H}}\boldsymbol{P}_{\mathrm{RF}}) + \\
&\quad \mathrm{tr}(\boldsymbol{P}_{\mathrm{B}}\boldsymbol{P}_{\mathrm{opt}}^{\mathrm{H}}\boldsymbol{P}_{\mathrm{opt}}\boldsymbol{P}_{\mathrm{B}}^{\mathrm{H}}) = \| \boldsymbol{P}_{\mathrm{opt}}\boldsymbol{P}_{\mathrm{B}}^{\mathrm{H}} - \boldsymbol{P}_{\mathrm{RF}} \|_{\mathrm{F}}^2
\end{aligned} \tag{14}$$

Finally, the upper bound is the objective function. To satisfy the power constraint in Eq. (8), it normalize $\boldsymbol{P}_{\mathrm{D}}$ by a factor of $\sqrt{N_s} / \| \boldsymbol{P}_{\mathrm{RF}}\boldsymbol{P}_{\mathrm{B}} \|_{\mathrm{F}}$ i. e., $\hat{\boldsymbol{P}}_{\mathrm{D}} = \sqrt{N_s}\boldsymbol{P}_{\mathrm{B}} / \| \boldsymbol{P}_{\mathrm{RF}}\boldsymbol{P}_{\mathrm{B}} \|_{\mathrm{F}}$. The following Theorem 1 will reveal the effect of this normalization.

Theorem 1 Suppose the Euclidean distance before normalization is $\| \boldsymbol{P}_{\mathrm{opt}} - \boldsymbol{P}_{\mathrm{RF}}\boldsymbol{P}_{\mathrm{D}} \|_{\mathrm{F}} \leqslant \delta$, δ represents the Euclidean distance, and after normalization it becomes $\| \boldsymbol{P}_{\mathrm{opt}} - \boldsymbol{P}_{\mathrm{RF}}\hat{\boldsymbol{P}}_{\mathrm{D}} \|_{\mathrm{F}} \leqslant 2\delta$.

Proof Define the normalization factor $\sqrt{N_s} / \| \boldsymbol{P}_{\mathrm{RF}}\boldsymbol{P}_{\mathrm{D}} \|_{\mathrm{F}} = 1/\psi$ and thus $\| \boldsymbol{P}_{\mathrm{RF}}\boldsymbol{P}_{\mathrm{D}} \|_{\mathrm{F}} = \psi\sqrt{N_s} = \psi \| \boldsymbol{P}_{\mathrm{opt}} \|_{\mathrm{F}}$.

By norm inequality, it can be obtained that

$$\| \boldsymbol{P}_{\mathrm{opt}} - \boldsymbol{P}_{\mathrm{RF}}\boldsymbol{P}_{\mathrm{D}} \|_{\mathrm{F}} \geqslant | \| \boldsymbol{P}_{\mathrm{opt}} \|_{\mathrm{F}} - \| \boldsymbol{P}_{\mathrm{RF}}\boldsymbol{P}_{\mathrm{D}} \|_{\mathrm{F}} | = |1 - \psi| \| \boldsymbol{P}_{\mathrm{opt}} \|_{\mathrm{F}} \tag{15}$$

Because $\| \boldsymbol{P}_{\mathrm{opt}} - \boldsymbol{P}_{\mathrm{RF}}\boldsymbol{P}_{\mathrm{D}} \|_{\mathrm{F}} \leqslant \delta$ and $\| \boldsymbol{P}_{\mathrm{opt}} - \boldsymbol{P}_{\mathrm{RF}}\boldsymbol{P}_{\mathrm{D}} \|_{\mathrm{F}} \geqslant |1 - \psi| \| \boldsymbol{P}_{\mathrm{opt}} \|_{\mathrm{F}}$, it can be obtained $\| \boldsymbol{P}_{\mathrm{opt}} \|_{\mathrm{F}} \leqslant \delta / |\psi - 1|$.

When $\psi \neq 1$, which indicates $\| \boldsymbol{P}_{\mathrm{opt}} - \boldsymbol{P}_{\mathrm{RF}}\boldsymbol{P}_{\mathrm{D}} \|_{\mathrm{F}} \neq 0$, $\| \boldsymbol{P}_{\mathrm{opt}} - \boldsymbol{P}_{\mathrm{RF}}\boldsymbol{P}_{\mathrm{D}} \|_{\mathrm{F}}$ can be rearranged as

$$\begin{aligned}
\| \boldsymbol{P}_{\mathrm{opt}} - \boldsymbol{P}_{\mathrm{RF}}\hat{\boldsymbol{P}}_{\mathrm{D}} \|_{\mathrm{F}} &= \left\| \boldsymbol{P}_{\mathrm{opt}} - \boldsymbol{P}_{\mathrm{RF}}\frac{\sqrt{N_s}}{\| \boldsymbol{P}_{\mathrm{RF}}\boldsymbol{P}_{\mathrm{D}} \|_{\mathrm{F}}}\boldsymbol{P}_{\mathrm{D}} \right\|_{\mathrm{F}} = \\
&\quad \left\| \boldsymbol{P}_{\mathrm{opt}} - \boldsymbol{P}_{\mathrm{RF}}\boldsymbol{P}_{\mathrm{D}} + \left(\boldsymbol{P}_{\mathrm{RF}}\boldsymbol{P}_{\mathrm{D}} - \frac{1}{\psi}\boldsymbol{P}_{\mathrm{RF}}\boldsymbol{P}_{\mathrm{D}} \right) \right\|_{\mathrm{F}} \leqslant \\
&\quad \| \boldsymbol{P}_{\mathrm{opt}} - \boldsymbol{P}_{\mathrm{RF}}\boldsymbol{P}_{\mathrm{D}} \|_{\mathrm{F}} + \left| \frac{\psi - 1}{\psi} \right| \| \boldsymbol{P}_{\mathrm{RF}}\boldsymbol{P}_{\mathrm{D}} \|_{\mathrm{F}} \leqslant \\
&\quad \delta + |\psi - 1| \| \boldsymbol{P}_{\mathrm{opt}} \|_{\mathrm{F}} \leqslant \\
&\quad \delta + \left| \frac{\psi - 1}{\psi - 1} \right| \delta = 2\delta
\end{aligned} \tag{16}$$

Proof end

Therefore, it has been proved that as long as the

Euclidean distance between the optimal digital precoder and the hybrid precoders is sufficiently small when ignoring the power constraint in Eq. (8), the normalization step will also achieve a small distance to the optimal digital precoder. With Eq. (14) serving as the objective function and the power constraint being temporarily lifted, the design issue for the hybrid precoder is redefined as

$$\left.\begin{aligned} &\min_{\boldsymbol{P}_{\mathrm{D}},\boldsymbol{P}_{\mathrm{RF}}} \| \boldsymbol{P}_{\mathrm{opt}}\boldsymbol{P}_{\mathrm{B}}^{\mathrm{H}} - \boldsymbol{P}_{\mathrm{RF}} \|_{\mathrm{F}}^{2} \\ &\text{s. t.} \\ &\quad P_{\mathrm{RF}m,n} \in \mathscr{A}; \quad \forall m,n \\ &\quad \boldsymbol{P}_{\mathrm{B}}^{\mathrm{H}}\boldsymbol{P}_{\mathrm{B}} = \boldsymbol{I}_{N_{\mathrm{s}}} \end{aligned}\right\} \tag{17}$$

The value of each PS is quantized to a set with a finite number of elements 2^B, which is expressed as $\mathscr{B} = \{ b\Delta \mid b = 0,1,2,\ldots,2^B - 1 \}$. B is the number of bits of resolution of PSs and $\Delta = (2\pi)/2^B$ is the quantization step size for a uniform quantizer, because of the practical implementation constraints of variable PSs. Accordingly, the elements of the analog precoder $\boldsymbol{P}_{\mathrm{RF}}$ are also limited. It denotes the constraint set of the analog precoder as $P_{\mathrm{RF}m,n} \in \mathscr{A} = \{ \exp(\mathrm{j}2\pi b/2^B) \mid b = 0,1,2,\ldots,2^B - 1 \}$. Obviously, a larger B will bring more finer resolution for the PSs and better performance, but it will also lead to higher hardware complexity and power consumption.

The objective function in Eq. (17) significantly simplifies the design of the analog precoder. The matrix $\boldsymbol{P}_{\mathrm{RF}}$ gets rid of the product form with $\boldsymbol{P}_{\mathrm{D}}$, a closed-form solution can be obtained as

$$\left.\begin{aligned} &\arg \boldsymbol{P}_{\mathrm{RF}} = \arg (\boldsymbol{P}_{\mathrm{opt}}\boldsymbol{P}_{\mathrm{B}}^{\mathrm{H}}) \\ &P_{\mathrm{RF}m,n} \in \mathscr{A}; \quad \forall m,n \end{aligned}\right\} \tag{18}$$

where $\arg \boldsymbol{P}_{\mathrm{RF}}$ generates a matrix containing the phases of the entries of $\boldsymbol{P}_{\mathrm{RF}}$. Thus, it shows that the phases of $\boldsymbol{P}_{\mathrm{RF}}$ can be extracted from the phases of an equivalent precoder $\boldsymbol{P}_{\mathrm{opt}}\ \boldsymbol{P}_{\mathrm{B}}^{\mathrm{H}}$. The FRPS algorithm for solving Eq. (17) is presented in Algorithm 1.

Algorithm 1 FRPS algorithm for solving Eq. (17)

Input: $\boldsymbol{P}_{\mathrm{opt}}$, B

1: Construct $\boldsymbol{P}_{\mathrm{RF}}^{(0)}$ with $\boldsymbol{P}_{\mathrm{RF}}^{(0)} = \boldsymbol{P}_{\mathrm{opt}}$ and set $k = 0$; $\boldsymbol{P}_{\mathrm{RF}}^{(0)}$ represents the initial value of $\boldsymbol{P}_{\mathrm{RF}}$.

2: for $k = 1$ to ε do

3: Fix $\boldsymbol{P}_{\mathrm{RF}}^{(k)}$ and $\boldsymbol{P}_{\mathrm{B}}^{(k)} = (\boldsymbol{P}_{\mathrm{RF}}^{(k)})^{\dagger}\boldsymbol{P}_{\mathrm{opt}}$;

4: Fix $\boldsymbol{P}_{\mathrm{B}}^{(k)}$, and $\arg \boldsymbol{P}_{\mathrm{RF}}^{(k+1)} = \arg (\boldsymbol{P}_{\mathrm{opt}}\boldsymbol{P}_{\mathrm{B}}^{(k)\mathrm{H}})$;

5: Construct $\mathscr{A} = \{ \exp(\mathrm{j}2\pi b/2^B) \mid b = 0,1,2,\ldots,2^B - 1 \}$;

6: Quantize $\boldsymbol{P}_{\mathrm{RF}}^{(k+1)}$ using $\mathscr{A}$;

7: end

8: For the digital precoder at the transmit end, normalize $\hat{\boldsymbol{P}}_{\mathrm{D}} = (\sqrt{N_{\mathrm{s}}}\boldsymbol{P}_{\mathrm{B}}) / \| \boldsymbol{P}_{\mathrm{RF}}\boldsymbol{P}_{\mathrm{B}} \|_{\mathrm{F}}$;

Output: $\boldsymbol{P}_{\mathrm{RF}}$, $\hat{\boldsymbol{P}}_{\mathrm{D}}$

In the FRPS algorithm, the dimension of the analog precoder is significantly higher than that of the digital precoder, leading to the complexity of the algorithm being chiefly generated by the analog part. During every cycle of the algorithm, the update of the analog precoder is executed through a phase extraction operation on the matrix $\boldsymbol{P}_{\mathrm{opt}}\boldsymbol{P}_{\mathrm{B}}^{\mathrm{H}}$, where the dimension of matrix $\boldsymbol{P}_{\mathrm{opt}}\boldsymbol{P}_{\mathrm{B}}^{\mathrm{H}}$ is $M_{\mathrm{T}} \times M_{\mathrm{T}}^{\mathrm{RF}}$, and the value of the analog precoder is quantized in a finite set of elements. The algorithm has low complexity. The algorithm calculates $\boldsymbol{P}_{\mathrm{D}} = \beta\boldsymbol{P}_{\mathrm{B}}$ in the last step, but this digital precoder should be normalized immediately. Therefore, the $\boldsymbol{P}_{\mathrm{B}}$ is normalized directly to satisfy the power constraint without knowing β. By looking at Eq. (6), it can be seen that the SE is not affected by β multiplied with $\boldsymbol{Q}_{\mathrm{D}}$. This is because both the received signals and noise have an effect on the $\boldsymbol{Q}_{\mathrm{D}}$, and thus the signal-to-noise ratio (SNR) is unaffected by the constant factor β. Besides, not having to calculate the constant β can result in a more streamlined algorithm.

To assess the tradeoff between the performance of the RF chain and the RF complexity in practice, based on the energy consumption model[29], it can specify the EE η as

$$\eta = \frac{R}{P_{\mathrm{total}}} = \frac{R}{P_{\mathrm{t}} + M_{\mathrm{T}}^{\mathrm{RF}}p_{\mathrm{RF}} + M_{\mathrm{PS}}p_{\mathrm{PS}}} \tag{19}$$

where P_{total} is the total energy consumption, R is the SE of the system, P_{t} is the transmitted energy, p_{RF} is the energy consumed by RF chain, p_{PS} is the energy consumed by PS. The number of PSs M_{PS} can be expressed as $M_{\mathrm{PS}} = M_{\mathrm{T}}M_{\mathrm{T}}^{\mathrm{RF}}$.

4 Simulation results and analysis

In this section, the simulation results related to SE and EE of the FRPS algorithm are presented. To

visually assess the performance of the FRPS algorithm, it is contrasted against the OMP [17] and phase extraction alternating minimization (PE-AltMin) hybrid algorithms[18]. Both OMP and PE-AltMin algorithms assume an infinite-resolution PS. Additionally, analog and fully digital precoding are also included in the simulation results for ease of comparison.

The parameters for the simulation are outlined below. Every t-VUE is equipped with $M_{\mathrm{T}}=144$ antenna elements. Every r-VUE is equipped with $M_{\mathrm{R}}=36$ antenna elements. The antenna elements in the UPA are separated by a half wavelength distance i. e., $d=\lambda/2$. A carrier frequency of 28 GHz is designated. Assume that r-VUE and t-VUE are moving at the same speed, $v^{\mathrm{Rx}}=v^{\mathrm{Tx}}=v=10$ m/s. The distance D between the two VUEs is 50 m. The channel matrix can be obtained based on the channel model described in Sect. 2. Clusters count is designated as $N_{\mathrm{C}}=5$, and the rays count within a single cluster is $N_{\mathrm{R}}=10$[18]. Clusters are endowed with equal power, i. e., $\sigma_{\alpha,i}^2=1$. The AoA and AoD are assumed to follow the uniform distribution within $[-\pi,\pi]$ and angular spread of $\pi/18$. The simulation encompasses 5 000 cycles in total.

It is set that the transmits energy $P_{\mathrm{t}}=1$ W[30], the energy consumed by RF chain $p_{\mathrm{RF}}=250$ mW[31] and SNR is 10 dB[32]. As the resolution of the PSs decreases, so does the power consumption. Based on the power linear decline model, the power consumption is 24 mW, 18 mW, 12 mW, and 6 mW for $B=4$ bit, $B=3$ bit, $B=2$ bit, and $B=1$ bit, respectively[32].

Fig. 2 depicts the influence of the PS resolution on SE. The assumption is made that the quantity of RF chains matches the quantity of data streams, i. e., $M_{\mathrm{T}}^{\mathrm{RF}}=M_{\mathrm{R}}^{\mathrm{RF}}=N_{\mathrm{s}}=2$. This represents the most adverse scenario, given that the count of RF chains is constrained to not fall below the levels stipulated in Sect. 2. It can be seen that with the PS resolution increasing, the SE will improve evidently within $B=3$ bit, which proves that the use of FRPS algorithm is beneficial for hybrid precoding schemes. It is observable that an augmentation in the quantity of transmitting antennas results in an enhancement of SE. It can be concluded that 3 bit resolution PS is sufficient for V2V systems using the FRPS algorithm. Compared with high-resolution PS, it offers a more cost-effective and less complex alternative for utilization.

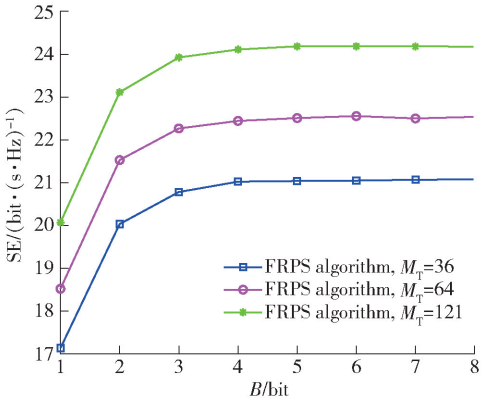

Fig. 2 SE vs. resolution of PS

Fig. 3 depicts the convergence characteristics of the FRPS algorithm. Assume that $M_{\mathrm{T}}^{\mathrm{RF}}=M_{\mathrm{R}}^{\mathrm{RF}}=N_s=2$ for the worst case.

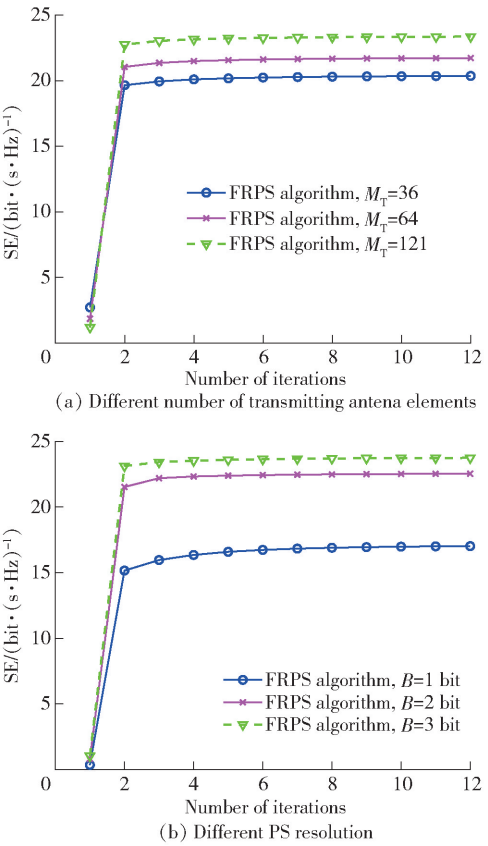

Fig. 3 SE vs. the number of iterations

The PS resolution $B=3$ bit are considered in

Fig. 3 (a). From Fig. 3 (a), it becomes clear that no matter how the number of antennas changes, the algorithm converges when the number of iterations is 2. As illustrated in Fig. 3 (b), the algorithm converges after 5 iterations with 1 bit resolution PS, after 3 iterations with 2 bit resolution PS and after 2 iterations with 3 bit resolution PS. This indicates that the FRPS algorithm has the capacity for swift convergence, which is a highly favorable property.

Fig. 4 depicts the SE against the SNR for different algorithms. The data stream $N_s = 2$ and $M_T^{RF} = M_R^{RF} = 4$ is considered. It can be seen that the SE of the FRPS algorithm with 3 bit resolution PSs is close to that of PE-AltMin algorithm with infinite-resolution PSs and even exceeds that of the OMP algorithm with infinite-resolution PSs. The algorithm is much better than the analog precoding algorithm. This is because the analog precoding can only control the signal phase, which brings performance loss. Additionally, it is noted that the FRPS algorithm secures over 90% of the SE of the fully digital precoding algorithm. Though fully digital precoding has the highest SE, it involves higher computational complexity and hardware requirements. It can be concluded that the FRPS algorithm is capable of enhancing the SE with smaller PSs resolution and lower computational complexity. This suggests that it can have greater precision close the performance of the existing infinite-resolution PSs algorithm, which can greatly save the hardware cost.

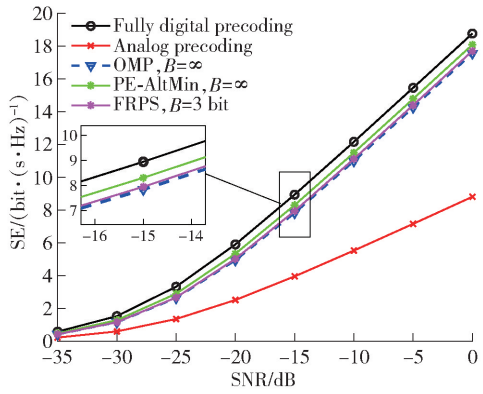

Fig. 4 SE achieved by different precoding algorithms

Fig. 5 depicts the SE versus the number of transmitting antennas. It is assumed that the data stream $N_s = 2$ and $M_T^{RF} = M_R^{RF} = 4$. The Rx is equipped with $M_R = 36$ antennas. Notably, as the number of antennas for transmission rises, there is a corresponding enhancement in SE. This is because the amplification of the quantities of antennas can provide more antenna diversity and greater interference immunity. Furthermore, the results indicate that the performance of the developed algorithm is close to that of the PE-AltMin algorithm and fully digital precoding strategies. It is gradually better than that of the OMP algorithm when the number of antennas is more than 100. It means that the performance of the FRPS algorithm is excellent as the number of transmitting antennas rises. The analysis shows that the SE of the analog precoding is lowest and grows slowly with the increase of the number of antennas, and the SE is much lower than that of other precoding algorithms. It can be concluded that the use of analog precoding is not feasible in the V2V system.

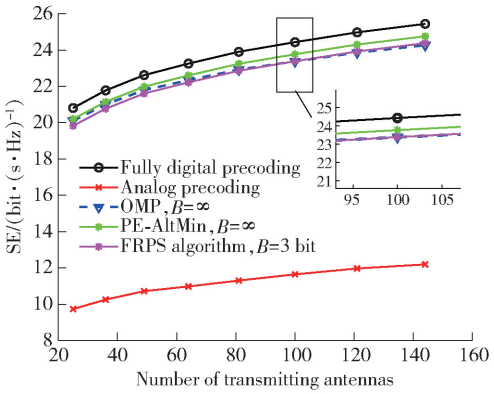

Fig. 5 SE vs. the number of transmitting antennas

Fig. 6 depicts the influence of the PS's resolution on EE.

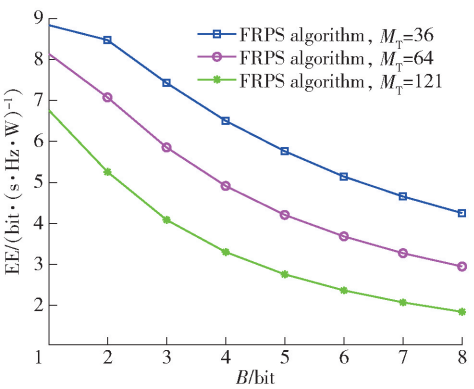

Fig. 6 EE vs. resolution of PS

It is assumed that $M_T^{RF} = M_R^{RF} = N_s = 2$ as Fig. 3 for the worst case. It can be observed that enhancing the resolution of the PS leads to a reduction in the EE. This means that the resolution of the PS cannot be blindly improved in the actual V2V system design. Additionally, the EE tends to decline with an escalating number of antennas utilized for transmission.

Fig. 7 depicts the EE versus the number of RF chains. The data stream $N_s = 2$ and $M_T^{RF} = M_R^{RF}$. It can be observed that the EE of the FRPS algorithm outperforms that of OMP, PE-AltMin, and fully digital precoding algorithms. Furthermore, it becomes clear that the EE of the FRPS algorithm when the RF chain is less than 3 is better than that of the analog precoding with one RF chain. It can be observed that the EE decreases with the increase of the RF chains with OMP, PE-AltMin, and the FRPS algorithm.

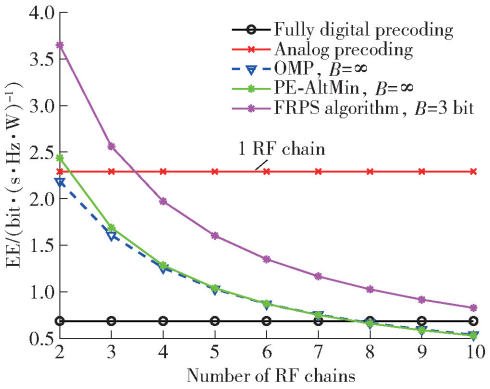

Fig. 7 EE vs. the number of RF chains

Fig. 8 depicts the EE versus the SE with different resolution of PSs. The data stream $N_s = 2$ and $M_T^{RF} = M_R^{RF} = 4$. It is shown that the V2V system performance improves as the resolution increases. However, although the improvement of resolution can make the phase quantization more accurate, the power consumption grows much faster than the SE with the increase of B, which leads to a sharp decline in EE. It implies that the use of infinite-resolution PSs in V2V system is not practical and causes large energy losses. The results in Fig. 8 further demonstrate the rationality of setting $B = 3$ bit for the FRPS algorithm. When $B >$ 3 bit, the SE will not increase significantly, but the EE will decrease significantly. Furthermore, observations indicate that with the increase of the number of transmitting antennas, the SE will increase but the EE will decrease.

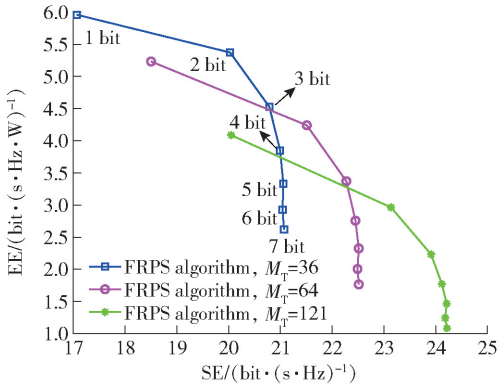

Fig. 8 EE vs. SE by different resolutions of PSs

Fig. 9 depicts the EE versus the SE with different numbers of RF chains. The data stream $N_s = M_T^{RF} = M_R^{RF}$. It can be seen that with the increase of RF chains, the SE of the V2V system increases, but the EE decreases. This is because the hardware and software complexity will increase with increasing the number of RF chains, which may lead to higher design and maintenance costs, and require more energy consumption.

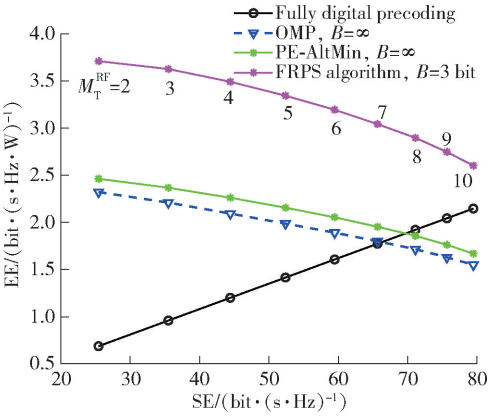

Fig. 9 EE vs. SE by different number of RF chains

By increasing RF chains, the signal can be controlled more accurately. The EE of the FRPS algorithm when $M_T^{RF} = M_R^{RF} = 10$ is even better than the PE-AltMin algorithm when $M_T^{RF} = M_R^{RF} = 2$. This means that when the same energy is consumed, the FRPS algorithm can achieve greater SE by setting more RF chains to make up for the loss caused by the insufficient resolution of the PSs. From the perspective

of both EE and SE, the FRPS algorithm is superior to other algorithms.

Fig. 10 depicts the EE versus the SE with different numbers of transmitting antennas. The data stream $N_s = 2$ and $M_T^{RF} = M_R^{RF} = 4$. It is observable that with increasing the number of transmitting antennas, the SE increases, but the EE decreases. It is clear that the FRPS algorithm performs excellently in terms of EE, approaching the lowest energy consumption with analog precoding regardless of the number of transmitting antennas.

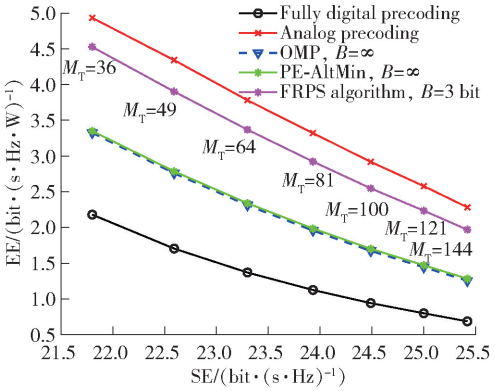

Fig. 10 EE vs. SE by different number of transmitting antennas

5 Conclusions

In this paper, a two-stage iterative hybrid precoding algorithm, FRPS, was proposed for the mmWave massive MIMO V2V system. The digital and analog precoders are jointly designed, and the discrete iterative optimization idea is used to solve the analog and digital precoders alternately. Numerical simulations confirm the effectiveness of the algorithm. As the data indicated, the FRPS algorithm demonstrates fast convergence and also approaches the SE of fully digital precoding with only 3 bit resolution PS. Moreover, the SE delivered by the FRPS algorithm outperforms the OMP algorithm and closely rivals the performance of the PE-AltMin algorithm. The EE of the FRPS algorithm outperforms the other infinite-resolution PS hybrid precoding algorithm and fully digital precoding algorithm.

Acknowledgements

This work was supported by the S&T Program of Hebei Province (2023KFKT002), the Natural Science Foundation of Hebei Province of China (F2024201053).

References

[1] SUN Y, HU Y F, ZHANG H, et al. A parallel emission regulatory framework for intelligent transportation systems and smart cities. IEEE Transactions on Intelligent Vehicles, 2023, 8(2): 1017 – 1020.

[2] NOOR-A-RAHIM M, LIU Z L, LEE H, et al. 6G for vehicle-to-everything (V2X) communications: enabling technologies, challenges, and opportunities. Proceedings of the IEEE, 2022, 110(6): 712 – 734.

[3] CHOWDHURY M Z, SHAHJALAL M, AHMED S, et al. 6G wireless communication systems: applications, requirements, technologies, challenges, and research directions. IEEE Open Journal of the Communications Society, 2020, 1: 957 – 975.

[4] BOGALE T E. Adaptive beamforming and modulation design for 5G V2I networks. Proceedings of the 10th Annual Computing and Communication Workshop and Conference (CCWC'20), 2020, Jan 6 – 8, Las Vegas, NV, USA. Piscataway, NJ, USA: IEEE, 2020: 90 – 96.

[5] LI C Y, FANG Y F, YU L J, et al. A 5G MmWave communication framework in vehicle-road cooperative system. Proceedings of the 8th Annual International Conference on Network and Information Systems for Computers (ICNISC'22), 2022, Sept 16 – 19, Hangzhou, China. Piscataway, NJ, USA: IEEE, 2022: 46 – 49.

[6] FU Z H, ZHANG Y, ZHAO X W, et al. A DNN-based channel state and scenario identifications for millimeter-wave communications. IEEE Transactions on Vehicular Technology, 2023, 72(6): 8088 – 8093.

[7] LI J, NIU Y, WU H, et al. Mobility support for millimeter wave communications: opportunities and challenges. IEEE Communications Surveys & Tutorials, 2022, 24(3): 1816 – 1842.

[8] CHUNG M K, LIU L, JOHANSSON A, et al. Millimeter-wave massive MIMO testbed with hybrid beamforming. Proceedings of the 54th Asilomar Conference on Signals, Systems, and Computers, 2020, Nov 1 – 4, Pacific Grove, CA, USA. Piscataway, NJ, USA: IEEE, 2020: 309 – 313.

[9] ZHANG J Y, BJÖRNSON E, MATTHAIOU M, et al. Prospective multiple antenna technologies for beyond 5G. IEEE Journal on Selected Areas in Communications, 2020, 38(8): 1637 – 1660.

[10] YOU L, CHEN X, SONG X H, et al. Network massive MIMO transmission over millimeter-wave and terahertz bands: mobility enhancement and blockage mitigation. IEEE Journal on Selected Areas in Communications, 2020, 38(12): 2946 – 2960.

[11] MORSALI A, CHAMPAGNE B. Achieving fully-digital performance by hybrid analog/digital beamforming in wide-band massive-MIMO systems. Proceedings of the 2020 IEEE International Conference on Acoustics, Speech and Signal Processing (ICASSP'20), 2020, May 4 – 8, Barcelona, Spain.

Piscataway, NJ, USA: IEEE, 2020: 5125 – 5129.
[12] GHEREKHLOO S, ARDAH K, HAARDT M. Hybrid beamforming design for downlink MU-MIMO-OFDM millimeter-wave systems. Proceedings of the IEEE 11th Sensor Array and Multichannel Signal Processing Workshop (SAM'20), 2020, Jun 8 – 11, Hangzhou, China. Piscataway, NJ, USA: IEEE, 2020: 5p.
[13] LIU F L, BAI X Y, DU R Y, et al. Adaptive hybrid precoding with high energy efficiency for millimeter wave communication systems. IEEE Systems Journal, 2022, 16(4): 5164 – 5175.
[14] GAUTAM P R, ZHANG L. Hybrid precoding for millimeter wave MIMO: trace optimization approach. IEEE Access, 2022, 10: 66874 – 66885.
[15] PANG L H, WU W J, ZHANG Y, et al. Joint power allocation and hybrid beamforming for downlink mmwave-NOMA systems. IEEE Transactions on Vehicular Technology, 2021, 70(10): 10173 – 10184.
[16] WANG S G, HE M Y, ZHANG Y J, et al. Joint hybrid precoding scheme with low complexity for single-user massive MIMO systems. Proceedings of the 2020 International Conferences on Internet of Things (iThings'20) and IEEE Green Computing and Communications (GreenCom'20) and IEEE Cyber, Physical and Social Computing (CPSCom'20) and IEEE Smart Data (SmartDat'20) and IEEE Congress on Cybermatics (Cybermatics'20), 2020, Nov 2 – 6, Rhodes, Greece. Piscataway, NJ, USA: IEEE, 2020: 175 – 179.
[17] EL AYACH O, RAJAGOPAL S, ABU-SURRA S, et al. Spatially sparse precoding in millimeter wave MIMO systems. IEEE Transactions on Wireless Communications, 2014, 13(3): 1499 – 1513.
[18] YU X H, SHEN J C, ZHANG J, et al. Alternating minimization algorithms for hybrid precoding in millimeter wave MIMO systems. IEEE Journal of Selected Topics in Signal Processing, 2016, 10(3): 485 – 500.
[19] SHABAN A W, DAMEN O, XIN Y, et al. Statistically-aided codebook-based hybrid precoding for millimeter wave channels. IEEE Access, 2020, 8: 101500 – 101513.
[20] LYU S, WANG Z, GAO Z, et al. Lattice-based mmWave hybrid beamforming. IEEE Transactions on Communications, 2021, 69(7): 4907 – 4920.
[21] KUO C H, CHANG H Y, CHANG R Y, et al. Unsupervised learning based hybrid beamforming with low-resolution phase shifters for MU-MIMO systems. Proceedings of the 2022 IEEE International Conference on Communications (ICC'22), 2022, May 16 – 20, Seoul, Republic of Korea. Piscataway, NJ, USA: IEEE, 2022: 425 – 431.
[22] WEN L Y, QIAN H, LI M Q, et al. QoS-guaranteed hybrid beamforming design for multi-user systems with finite-resolution phase shifters. IEEE Transactions on Green Communications and Networking, 2023, 7(4): 1678 – 1691
[23] WANG Z H, LI M, LIU Q, et al. Hybrid precoder and combiner design with low-resolution phase shifters in mmWave MIMO systems. IEEE Journal of Selected Topics in Signal Processing, 2018, 12(2): 256 – 269.
[24] DU J B, XU W, DENG Y S, et al. Energy-saving UAV-assisted multiuser communications with massive MIMO hybrid beamforming. IEEE Communications Letters, 2020, 24(5): 1100 – 1104.
[25] LEE Y, LEE J H, KO Y C. Beamforming optimization for IRS-assisted mmWave V2I communication systems via reinforcement learning. IEEE Access, 2022, 10: 60521 – 60533.
[26] ZUGNO T, DRAGO M, GIORDANI M, et al. NR V2X communications at millimeter waves: an end-to-end performance evaluation. Proceedings of the 2020 IEEE Global Communications Conferencee (GLOBECOM'20), 2020, Dec 7 – 11, Taipei, China. Piscataway, NJ, USA: IEEE, 2020: 6p.
[27] LOTA J, JU S H, KANHERE O, et al. MmWave V2V localization in MU-MIMO hybrid beamforming. IEEE Open Journal of Vehicular Technology, 2022, 3: 210 – 220.
[28] WANG X, KONG L H, KONG F X, et al. Millimeter wave communication: a comprehensive survey. IEEE Communications Surveys & Tutorials, 2018, 20(3): 1616 – 1653.
[29] GAO X Y, DAI L L, HAN S F, et al. Energy-efficient hybrid analog and digital precoding for mmWave MIMO systems with large antenna arrays. IEEE Journal on Selected Areas in Communications, 2016, 34(4): 998 – 1009.
[30] RAPPAPORT T S, MURDOCK J N, GUTIERREZ F. State of the art in 60-GHz integrated circuits and systems for wireless communications. Proceedings of the IEEE, 2011, 99(8): 1390 – 1436.
[31] AMADORI P V, MASOUROS C. Low RF-complexity millimeter-wave beamspace-MIMO systems by beam selection. IEEE Transactions on Communications, 2015, 63(6): 2212 – 2223.
[32] CHEN C, DONG Y, CHENG X, et al. Low-resolution PSs based hybrid precoding for multiuser communication systems. IEEE Transactions on Vehicular Technology, 2018, 67(7): 6037 – 6047.

(Editor: Wang Xuying)